Special Issue

http://dx.doi.org/10.3786/sincs2011.02

NANO-MICRO LETTERS ARTICLE

www.nmletters.org

(Proceedings of 2011 Shanghai International Nanotechnology Cooperation Symposium, SINCS 2011, Published online 10 January 2012)

A Simple Hydrothermal Synthesis of Shape-controlled CeO_2 Nanomaterials

G. L. Tao, X. L. Lu, Z. H. Su, Y. Tao, H. P. Wu*

Abstract: Here we report a simple hydrothermal method to prepare shape-controlled nanoceria. By simply varying the reaction time and the concentration of $Ce(NO_3)_3$ in the reaction system, ceria nanomaterials with different morphologies such as nanoparticles, nanorods and nanowires could be obtained in the final products. UV–vis spectrum measurements were used to check the absorption abilities of these nano-sized ceria materials. PL spectrum illustrated the intensities of emission peak at 400 nm would increase sharply when the morphology of ceria changed from nanoparticles to nanowires, which is caused by the increasing of oxygen vacancy in the samples. A possible crystal growth mechanism was put forward based on the in-situ observation of UV absorptions.

Keywords:

Citation: G. L. Tao, X. L. Lu, Z. H. Su, Y. Tao and H. P. Wu, "A Simple Hydrothermal Synthesis of Shape-controlled CeO_2 Nanomaterials", Proceedings of Shanghai International Nanotechnology Cooperation Symposium, 5-9 (2011). http://dx.doi.org/10.3786/sincs2011.02

Introduction

Controllable synthesis of inorganic nanocrystal morphology is one of the most important topics in the field of advanced materials because of their shape- and size-dependent materials properties. CeO_2, an important technological material, it exhibits a large capacity for the storage of oxygen [1,2] (OSC) and serves as a solid electrolyte or anode material in solid-oxide fuel cells [3], oxygen sensor, ultraviolet absorber [4,5], and catalyst for various reactions. Stimulated by both the promising applications and the fantastic properties, many effects have been focused on the controlled synthesis of CeO_2 nanostructured materials. Shape-controlled ceria were prepared using various methods such as hydrothermal [6-10], reversed micelles [11-14], sol-gel [15], precipitate [16-18], sonochemical [19], Pyrolysis. Among them, hydrothermal method is regarded as an effective process due to its low reaction temperature and simple process. Recently, much attention was paid to simplify the process of hydrothermal [20,21]. Unlike common hydrothermal process, here we just use H_2O_2 as solvent and oxide reagent, $Ce(NO_3)_3{\cdot}6H_2O$ as cerium resource. No template or surfactant was introduced. Both shape and size of the ceria nanomaterial could be adjusted by varying reaction time and concentration of cerium in solution. Nano-sized ceria with good disperse can directly precipitate on the bottom of autoclave, no centrifugation and washing process were need after reaction. A possible growth mechanism of CeO_2 nanocrystals was put forward to explain the growth process based on the detail analysis of the growth process.

Exprimental section

Preparation of nanosized cerium oxide with different morphologies

Chemical reagents including $Ce(NO_3)_3{\cdot}6H_2O$, H_2O_2 and toluene were used as received without purification. In a typical experiment, 20 ml of 0.1 mol/L $Ce(NO_3)_3$ H_2O_2 solution was transferred into a 50 ml Teflon-lined

Department of Materials Science and Engineering, Changzhou University, Changzhou 213163, China
*Corresponding author. E-mail: 10409011@zju.edu.cn

stainless-steel autoclave, and 15 ml toluene were added into the autoclave in the ambient temperature without stirring. Controlling reacted for 4 h at 160℃, after reaction, obtained products directly precipitated on the bottom of autoclave. These nanomaterials could be directly dispersed in ethanol after removing the upper solution. The products were dried in oven for 24 h under 80℃ before characterization.

Characterizations

Specimens for transmission electron microscopy (TEM JEOL-2010) were prepared by dispersing the solid powder in ethanol and then dipping the solution onto a carbon-coated copper grid. Field Emission Scanning electron microscopy (FESEM) measurements were carried out on a LEO 1450 VP and the specimens were prepared by bonding solid power onto a alumina substrate with conductive adhesive tape. X-ray powder diffraction (XRD) measurements were performed using a Rigaku D/MAX-2550PC X-ray powder diffractometer with Bragg-Brentano geometry using Cu K_α irradiation in the range of 20-80 degrees, a step of 0.05 degree and 2 s per step. The UV-Vis spectra of the samples were recorded on a Cary 100a UV-Vis spectrophotometer using a quartz cell (1 cm path length). The wavelength ranged from 200 to 800 nm and the distance is 1 nm. Pure ethanol was used as background in the UV-Vis absorption spectra measurements, and the specimens were prepared by dispersing solid powder into ethanol with a concentration of 10^{-3} mol/l. PL measurements were carried out at room temperature using a SRenishaw in Via laser Raman spectrum.

Results and discussions

XRD characterization for ceria nanocrystals with different morphologies

The phases and purities of the as-prepared samples were investigated by XRD analysis. Figure 1 shows XRD patterns for CeO_2 with different shapes. All diffraction peaks can be indexed according to a face-centered cubic-phase (PCPDF34-0394), no other impurities were detected. It is noticed the ratio of intensity of $I_{(200)}/I_{(111)}$ increased as the appearance and growth of rod-like ceria, which means nanorods grew along the direction of [200] as reported in [22,23].

TEM and SEM observations for ceria nanocrystals with different shapes

The detailed formation process of CeO_2 nanostructures was examined by TEM. Figure 2(a) is the TEM image of CeO_2 nanoparticles sample prepared for 2 hours. It reveals that the sizes of these particles are about 5 nm, and part of them show cube-like shape. As the reaction time increasing, nanorods appeared in the products, Fig. 2(b) shows the TEM image of the products obtained after 4 hours reaction. There are nanoparticles and nanorods included in the products. It shows the similar size bewteen nanoparticles and diameters of nanorods, which means the nanorods come from oriented attachment of nanoparticles. Nanorods are the main shape when reaction time increased 24 hours, which can be found in Fig. 2(c). These nanorods have typical diameters of about 5-8 nm and lengths up

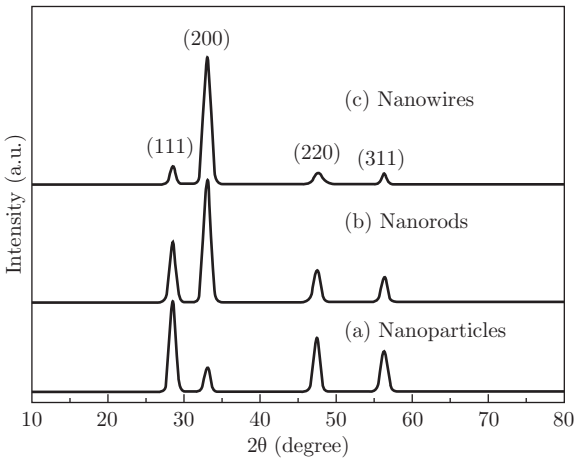

Fig. 1 XRD patterns for Ceria nano-particles, nano-rods and nanowires.

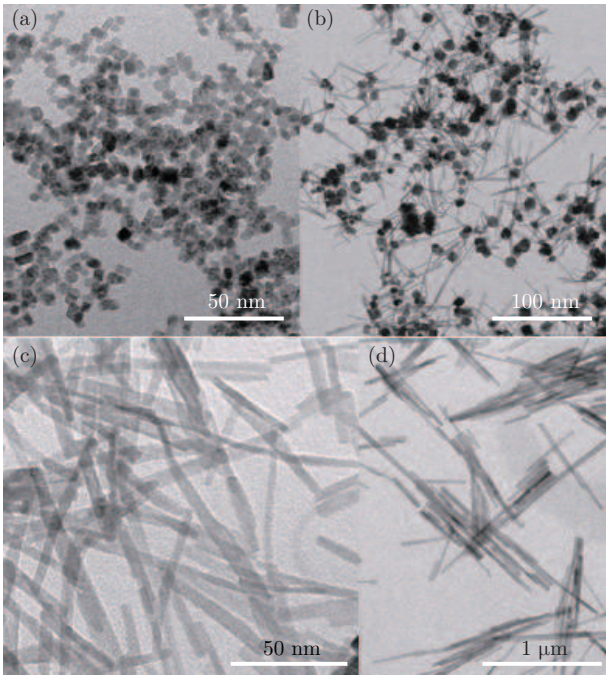

Fig. 2 (a) Ceria nanoparticles with size of 5nm obtained by reacting for 2 hour; (b) TEM image of nanopaticles and nanorods obtained by reacting for 4 hous; (c) TEM image of nanorods by reacting for 24 hours; (d) TEM image of nanowires with length of 1μm obtained for reacting 72 hours.

to 100 nm, and show a perfect circular cross section perpendicular to its axis. Further increasing the reaction time to 72 h, nanorods would change into nanowires. Figure 2(d) is the TEM image of CeO_2 nanowires with length of 1 μm. It implies these nanowires show small aspect ratios, which indicates the growth direction did not change during nanorods grew into nanowires.

Figure 3 is the TEM and FESEM images of ceria prepared as varying the concentration of $Ce(NO_3)_3$ solution increased from 5 g/L to 16 g/L, and the reaction time kept at 24 hours. Form it we can find that the amount of short rods will decrease with increasing the concentration of $Ce(NO_3)_3$. These nanorods assembled into perfect nanocubes during reaction process. These nanocubes are built up by nanorods and nanowires which can clearly find in FESEM image (Fig. 3d). Previous studies also reported the similar process [24,25].

UV-vis observations for ceria nanocrystals with different shapes

UV–vis spectrum measurements can also be used to track the morphological evolution during the growth process of the CeO_2 nanocrystals because CeO_2 nanocrystals with different shapes and sizes exhibit different band gap energies. The optical absorption spectrums for CeO_2 dispersed in ethanol are shown in Fig. 4. A sharp strong absorption peak was found at 208 nm. For different nanomaterials, no sharply shifts are found when the reaction time increases. The other absorption peak located at 260 nm. The intensity of 260 nm peak will increase when the morphology of ceria changed from nanoparticles to nanowires, which was caused by higher oxygen vacancy concentration in fibre-like products.

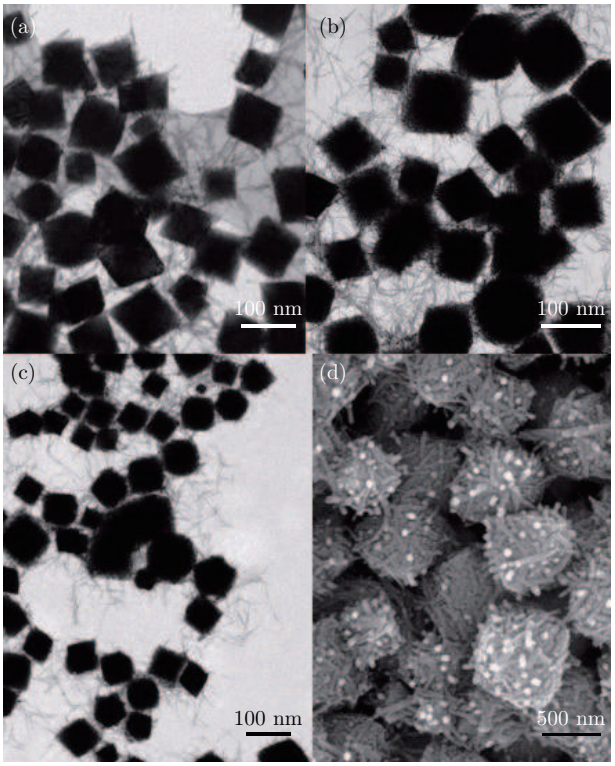

Fig. 3 (a)∼(c) TEM images of nanorods by varying the concentration of $Ce(NO_3)_3$ from 5 g/L, 5.5 g/L to 6 g/L; (d) FESEM image of some cube shaped CeO_2 composed by CeO_2 nanorods.

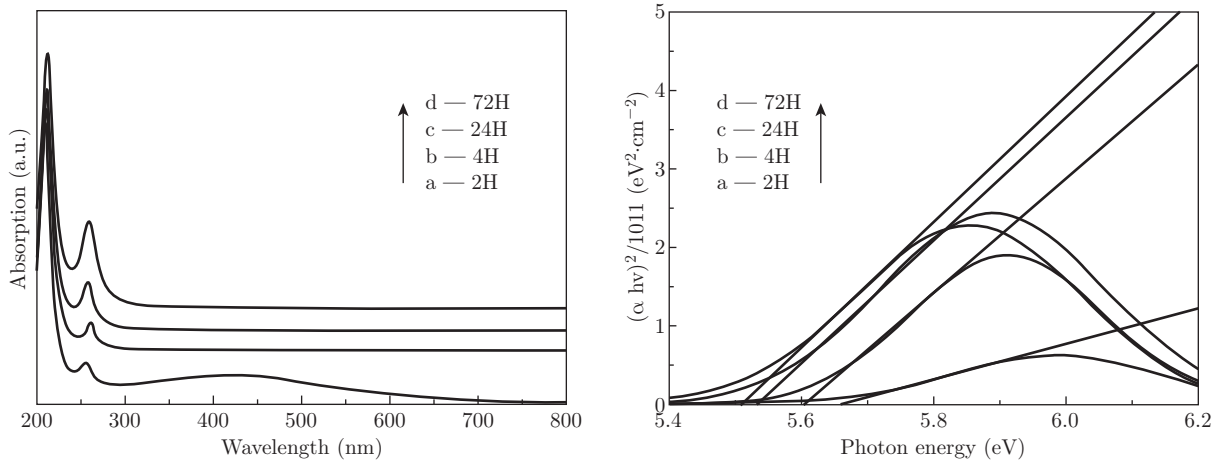

Fig. 4 (a) UV spectra for CeO_2 nanocrystals prepared under different reaction time. (b) The plots of $(\alpha hv)^2$ *vs* photon energy for the samples prepared with different reaction time.

To reveal the relationship between band gap energies and morphologies of the samples, the direct band gap energy (E_g) for the ceria nanmaterials with different aspect ratio was determined by fitting the absorption data to the direct transition equation:

$$\alpha hv = A(hv - E_g)^{1/2}$$

where α is the absorption coefficient, hv is the photon energy, E_g is the direct band gap and A is a constant.

The absorption coefficient (α) is defined as:

$$\alpha = \frac{2.303 \times 10^3 A\rho}{Lc}$$

where A is the absorbance of the sample, ρ is the real density of CeO_2 (7.28 g/cm^{-3}), L is the path length of the quartz cell (1 cm), and c is the concentration of the ceria suspensions (CeO_2 were dispersed in toluene). The plots of $(\alpha hv)^2$ *VS* hv are shown in Fig. 4(b).

The absorption of CeO_2 in the UV range originates from the charge-transfer between the O 2p and Ce 4f states in O^{2-} and Ce^{4+}. From the intersection of the extrapolated linear portion, the E_g values of the CeO_2 can be determined as 5.66, 5.61 and 5.51 eV respectively. It indicates that the band gap decreased as morphological evolution.

PL observations for ceria nanocrystals with different shapes

Room temperature PL spectrum of the CeO_2samples with different shapes is shown in Fig. 5. It illustrates strong green emission band near 600 nm for all samples which could be explained by charge transition between 4f band and valence band. It indicates the intensity of intrinsic peak decreased as the the reaction increased. Another emission peak appeared at 350 nm. Form it we can find that the relative intensity of the peak near 400 nm increased as the aspect ratio of the nanoparticles increased. The possible from two sides, on one hand, the concentration of oxygen vacancies increased during longer time reaction, on the other side, the defect levels localized between the Ce 4f band and the O 2p band also can result in weak emission bands [26,27].

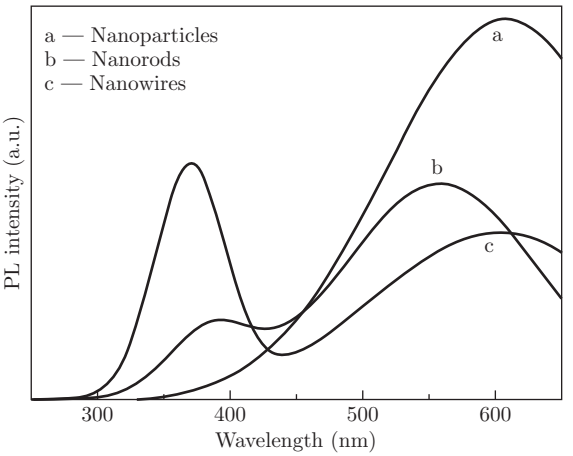

Fig. 5 PL spectra for nanoparticles, nanorods and nanowires.

The growth mechanism for ceria nanocrystals

The morphologies and sizes of CeO_2 nanocrystals obtained in different reaction condition show irradiation time-dependent evolution. Based on TEM and XRD characterizations, a possible growth mechanism for the morphologies evolution was put forward as nucleation-oriented attachment-grow. Schematic is shown in Fig. 6. Firstly, the oxidation reaction of Ce from Ce^{3+} to Ce^{4+} happens with OH- and O_2 generated from H_2O_2. These Ce(IV) will decompose under 160℃ as shown in following:

$2H_2O_2 \rightarrow 2H_2O + O_2$

$4Ce^{3+} + O_2 + 2H_2O \rightarrow 4Ce^{4+} + 4OH^-$

$4Ce^{4+} + 4OH^- \rightarrow Ce(OH)_4$

$Ce(OH)_4 \rightarrow CeO_2 + 2H_2O$

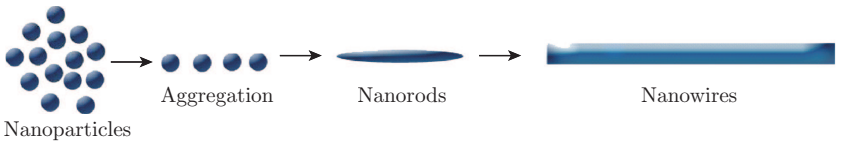

Fig. 6 Schematic illustration of the growth mechanism for CeO_2.

In the early stage, these CeO_2 nucleus grow and aggregate to form CeO_2 nanoparticles which is caused by Ostwald ripening. CeO_2 nanorods can be obtained in the system after 4 hours reaction, which come from the oriented attachment of nanoparticles. These nanorods assemble and grow along [100] direction, as demonstrated by XRD result. In particular, the (100) surface is a "type III" surface, and there is a dipole moment perpendicular to the surface, which means its surface energy diverges and the structure is considered less stable. So it is much easier to grow along [100] than any other directions as reported in [28]. Usually, the crystals were easy to form symmetry cubic morphology and reduce the overall surface energy of the system, so they choose the growth direction along the lowest energy direction. The growth of CeO_2 nanowires was based on the growth of CeO_2 nanorods along (100) direction.

Conclusions

In summary, a simple synthesis method was developed by using simply raw materials and reaction process, ceria nanomaterials with different morphologies and sizes can be obtained by varying the reaction and the concentration of $Ce(NO_3)_3$ in the system. A possible growth mechanism of CeO_2 nanowires was put forward as nucleation-oriented attachment-grow.

References

[1] D. Zhang, H. Fu, L. Shi, C. Pan, Q. Li , Y. Chu and W. Yu, Inorganic Chem, Vol. 46, No. 7, pp 2446-2451 (2007).

[2] C. Campbell, Peden C, Science, Vol. 309, pp713-714 (2005).

[3] Y. Zhang, S. Zha, and M. Liu, Advanced Materials, Vol. 17, No. 4, pp487-491 (2005).

[4] T. Masui, K. Fujiwara, K. Machida and Adachi G, Chemistry Materials. Vol. 9, No. 10, pp2197-2204 (1997).

[5] A. Vantomme, Z. Y. Yuan, G. H. Du and B. L. Su, Langmuir, Vol. 21, No. 3, pp1132-1146 (2005).

[6] W. S. Yang and L. Gao, J. of Ame Chem Soc, Vol. 128, No. 28, pp9330-9331 (2006).

[7] C. S. Pan, D. S. Zhang and L. Y. Shi, J. Solid State Chem., Vol. 181, No. 6, pp1298-1302 (2008).

[8] M. Hirano and E. Kato, J. Ameriacan Chem Soc, Vol.79, No.3, pp777-780 (1996).

[9] K. Kenji, I. Koji and F. Bert, 2007. Structural and morphological characterization of cerium oxide nanocrystals prepared by hydrothermal synthesis. Nano Letter, Vol.7, No.2, pp421-425

[10] T. Masui, K. Fujiwara, K. I. Machida and G. Y. Adachi, Chem Mat, Vol. 18, No. 16, pp3808-3812 (2006).

[11] A. I. Y. Tok, F. Y. C. Boey and Z. Dong, J. Mat Processing Tech, Vol. 190, No. (1-3), pp217-222 (2007).

[12] J. Zhang, X. Ju, Z. Y. Wu, T. Liu, D. Hu and N. Y. Xie, Chem Mat, Vol. 13, No. 11, pp4192-4197 (2001).

[13] T. Masui, K. Fujiwara, K. Machida and G. Adachi, Chem Mater, Vol. 9, No. 10, pp2197-2204 (1997).

[14] K. Emanuel, S. Christian and G. Anett, J. Sol. Sta. Chem.,Vol. 181, No. 7, pp1614-1620 (2008).

[15] L. R. Christel, W. L. Jeffrey, A. Katherine, R. M. Pettigrew, M. S. Stroud and R. R. Debra, Chem Mater, Vol. 18, No. 1, pp 50-58 (2006).

[16] I. Ch. Huey and Y. Ch. Hung, Colloids and Surfaces A: Physicochemical and Engineering Aspects, Vol. 31, No. (1-3), pp61-69 (2005).

[17] T. Ming, Mater Sci Engineering B, Vol. 110, No. 2, pp132-134 (2004).

[18] I. Ch. Huey and Y. Ch. Hung, Sol. Sta. Commun., Vol. 133, No. 9, pp593-598 (2005).

[19] L. Yin, Y. Wang, G. Pang, Y. Koltypin and A. Gedanken, J. Colloid. Interf Sci, Vol. 246, No. 1, 78-94 (2002).

[20] Z. J. Yang, D. Q. Han, D. L. Ma, H. Liang and L. Liu, Cryst Growth and Design, Vol. 10, No. 1, 291-295 (2010).

[21] Y. Lai , R. B. Yu, J. Chen and X. R. Xing, Cryst Growth and Design, Vol. 8, No. 5, 1471-1477 (2008).

[22] M. Nogami, R. Koike, R. Jalem, G. Kawamura, Y. Yang and Y. Sasaki, Phys Chem Lett, Vol. 1, No. 2, 568-571.2010

[23] R. R. Cui, W. C. Lu , L. M. Zhang, B. H. Yue and S. S. Shen, J. Phys Chem C, Vol. 113, No. 52, 21520-21525 (2009).

[24] G. Zh. Chen, C. C. Xu, X. Y. Song, Sh. L. Xu, Y. Ding and S. X. Sun, Cryst Grow & Design, Vol. 8, No. 12, 4449 (2008).

[25] C. Sun, H. Li, H. Zhang, Z. Wang and L. Chen, Nanotech, Vol. 16, No. 9, 1454 (2005).

[26] Ch. W. Sun, H. Li and Chen L Q, 2007. Study of flowerlike CeO2 microspheres used as catalyst supports for CO oxidation reaction. Journal of Chemistry Physics Solids, Vol. 68, No. 9, pp1785-1790.

[27] M. Y. Chen, Z. T. Zu , X. Xiang. and H. L. Zhang, Phys B, Vol. 389, No. 2, 263 (2007).

[28] S. C. Kuiry, S. Patil, S. Deshpande and S. Seal, J. Phys Chem B, Vol. 109, No. 15, 6936 (2005).